Solid Freeform Fabrication 2016: Proceedings of the 27th Annual International Solid Freeform Fabrication Symposium – An Additive Manufacturing Conference
Reviewed Paper

IN-SITU PROCESS MONITORING AND EX-SITU PART QUALITY ASSESSMENT OF SELECTIVE LASER SINTERING USING OPTICAL COHERENCE TOMOGRAPHY

Adam Lewis[1], Michael Gardner[2], Austin McElroy[2], Thomas Milner[2], Scott Fish[3], Joseph Beaman[3]

[1]McKetta Department of Chemical Engineering
[2]Department of Biomedical Engineering
[3]Department of Mechanical Engineering
Cockrell School of Engineering, The University of Texas at Austin, Austin, TX 78705

Abstract

Widespread commercial adoption of Selective Laser Sintering has been hindered by inadequate quality and consistency of manufactured parts. Improved process monitoring and control have the potential to improve part quality and thus increase adoption of SLS for various applications. In this paper, optical coherence tomography (OCT) is explored as a new process monitoring tool in SLS polymer printing. The basic operating principles behind OCT are reviewed to illustrate the potential monitoring capabilities followed by results for both in-situ process monitoring and ex-situ examinations of built parts comprised of various polymers. Capabilities and limitations of OCT in each application are discussed.

Introduction

The Additive Manufacturing (AM) industry continues to expand rapidly, growing by over US $1 billion for the 2nd year in a row with a 2016 growth rate (CAGR) of 25.9% [1]. Selective Laser Sintering (SLS) is one of the earliest AM techniques and continues to gain further use in prototyping and end-use applications in the medical and aviation industries among others [2]. However, SLS manufactured parts continue to be plagued with irregular surface quality and inconsistent strength and dimensions among other issues. In large part, these problems can be attributed to the lack of process monitoring tools in SLS machines. The extent of monitoring in most commercial SLS machines consists of data acquired from a few thermocouples and pyrometers during operation. New and/or improved process monitoring tools coupled with control strategies can help reduce many of the part quality issues mentioned. In this paper Optical coherence tomography (OCT) is presented as a new process monitoring tool with the ability to provide information not accessible through traditional SLS process monitoring methods.

Principles of Optical Coherence Tomography

Optical coherence tomography (OCT) is an established medical imaging technique based on low coherence interferometry commonly used in biomedical optics and medicine. OCT is used in this field and others for its ability to provide subsurface visualization of translucent or turbid materials. OCT produces cross-sectional and volumetric images from magnitude and echo time delay data of backscattered radiation. Samples can be imaged in real time with typical axial resolutions of 1-15 microns.

A single OCT scan at a point on the surface of the sample, is known as an A-scan and yields depth information at this point. A collection of subsequent A-scans is called a B-scan and yields cross sectional information for the sample. Subsequent B-scans can be combined to yield a 3D representation of the sample as shown in Figure 1 [3].

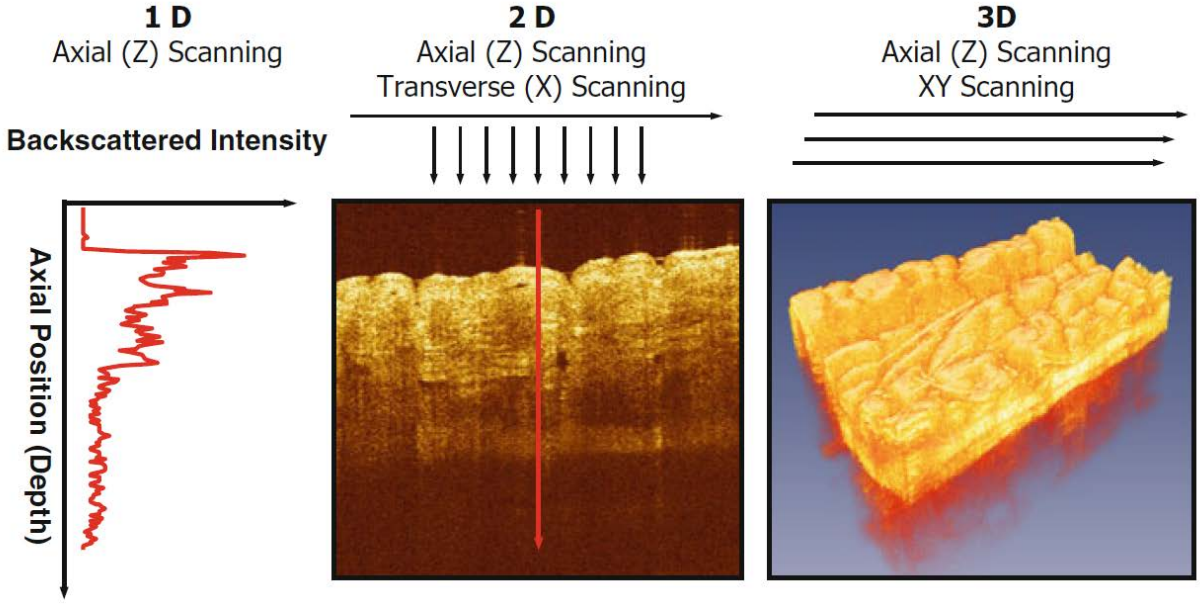

Figure 1 (Left) A single A-scan is shown. (Middle) A cross sectional B-scan is shown with intensity data shown in false color. (Right) Many B-scans have been combined to form a volumetric rendering of the sample. [3]

Figure 2 illustrates some basic OCT concepts. In OCT, light from a laser is split into "sample" and "reference" beams. The reference beam is split from the source light and serves as a reference time delay for light returning from the sample. The sample beam is forward scattered and possibly absorbed as it propagates into the media of interest. Some radiation entering the sample is backscattered and re-combines with the reference beam forming an interference between these beams that is measured by a photodetector. From this measurement, spatial information about the sample can be obtained. Interfaces where the index of refraction changes suddenly (large longitudinal gradient), including variations in material phase and material type are often detectable with OCT.

There are several different types of OCT systems. An optical fiber-based swept source OCT system (SS-OCT) was used for the experiments in this paper. Detailed information about other types of OCT can be found in [3]. Additional SS-OCT specific background information is provided below.

In SS-OCT systems, the wavelength of the radiation emitted by the laser changes in time as it sweeps across a frequency range during each A-scan. The light in the sample arm is configured to travel slightly longer than that in the reference arm. The difference in pathlength between light in reference and sample paths causes the phase of the interference fringes to vary as the optical source frequency (ν) varies. The phase (ϕ) of the interference between reference and sample paths varies as $\phi = 2\pi c \tau \nu$ where c is the speed of light ν is the optical frequency and τ is the time delay between sample and reference paths. Because light in the sample beam travels variable path length delays (τ) depending on how far into the sample it penetrates before back

reflecting, a Fourier transformation is necessary to allow the individual path length delays in the interference signal to be separated out yielding the axial scan information (echo magnitude vs. time delay).

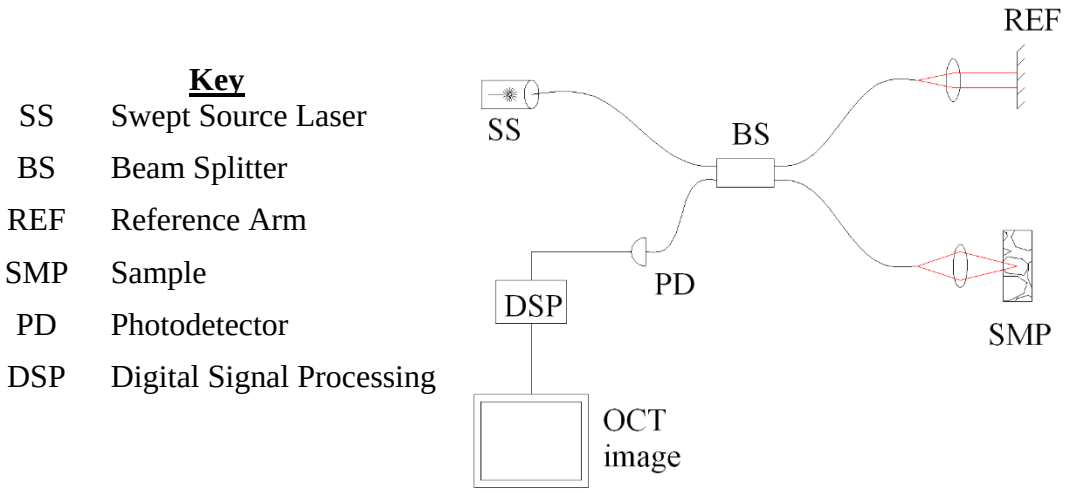

Figure 2: A schematic of a simple two-beam swept source OCT system (SS-OCT) [4]

Stifter reviews several applications of OCT which including inspection of polymeric injection molded parts of polyamide and PEEK materials [5]. Quite recently, OCT was used for ex-situ analysis of SLS manufactured parts by Guan et.al. [6]; however, to the authors' knowledge OCT has not been used as a process monitoring tool during an SLS build. In this paper, OCT is investigated as a tool for in-situ process monitoring during the selective laser sintering of nylon 12. To this end, ex-situ analysis was first performed to verify the feasibility of OCT for in-situ process monitoring.

Ex-Situ Part Examination: Experimental Setup

For the ex-situ part imaging, the OCT system used a commercially available 30 mW AXSUN swept source laser with a center wavelength of 1310nm and a wavelength tuning range of 125nm at a 100 kHz sweep rate. The axial scan resolution is approximately 3.75 μm/pixel in air and the lateral resolution is approximately 16 μm/pixel. The maximum scan depth is approximately 4 mm in air. Each B-scan is made up of 512 A-scans. All of the parts imaged for the ex-situ part examination were built in UT Austin's Laser Additive Manufacturing Pilot System (LAMPS) machine. The LAMPS machine was developed at UT Austin for the study of SLS process control in high melting-point temperature polymers [9]. A more detailed description of the LAMPS machine is provided later in this paper.

Ex-Situ Part Examination: Results

The following selectively laser sintered parts were imaged as part of the preliminary ex situ OCT analysis: a nylon 12 tensile bar specimen with a ledge, half of a nylon tensile bar specimen in which layering was visible, and a PEEK part with noticeable surface pitting.

Nylon 12 Tensile Bar w/ Ledge

First, a nylon 12 part with a ledge was imaged. The ledge was created inadvertently as the SLS powder roller moved the previously sintered layers slightly while spreading subsequent powder layers. This part was selected because the ledge allows one to ascertain if the OCT system is able to penetrate through a few layers of the material before the backscattering of the laser is indistinguishable from noise. Figure 3 shows visual images of the described part.

Figure 3: (Left) View of tensile bar from above (Right) The ledge is apparent on the left of the image when looking at the tensile bar from the end.

Figure 4 shows the B-scan cross section of the tip of the ledge. The bottom boundary of the ledge is clear up to at least the red dotted line in Figure 5, which is approximately 0.36 mm or 3.6 layers in this particular part. Because this was merely a feasibility study in preparation for the in-situ analysis, and did not include surrounding un-melted powder, precise criteria were not used to identify the maximum depth of resolution of this ledge. The surface depth is assumed to be indicated by the local maximum of intensity values versus depth in each A-scan. In absence of a measurement, the index of refraction of the sintered material was assumed to be 1.53 and 1.00 for the air [7].

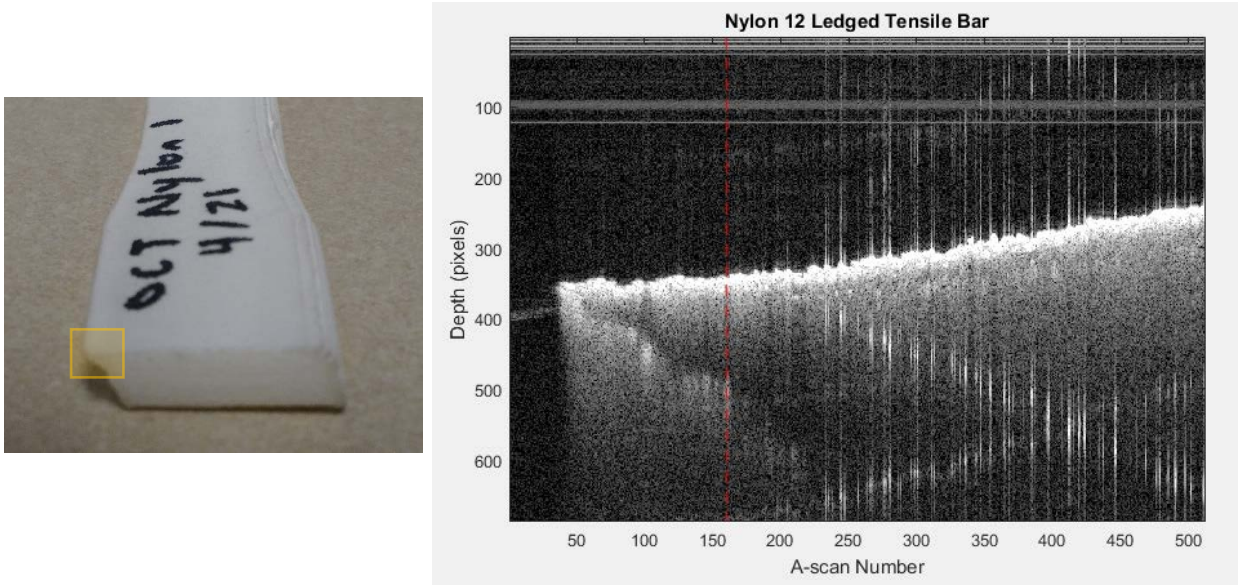

Figure 4: (Left) A visual image is provided for reference with the approximate region of the OCT scan indicated by the square. (Right) A single B-scan of the tensile bar ledge is shown.

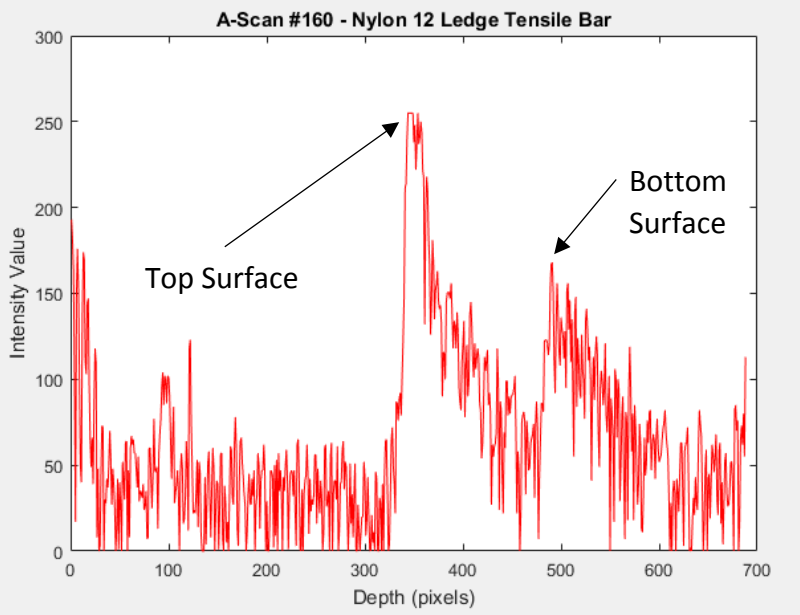

Figure 5: A scaled intensity value from a single A-scan is shown with the top and bottom surfaces sintered parts are indicated.

Half of Nylon 12 Tensile Bar

A half of a nylon 12 tensile bar specimen was also imaged. Layering was visible by eye on the outside of the part. Layering was also visible using OCT. Figure 6 shows a visual image of the part described. Figure 7 shows the OCT image of the layered half tensile bar and Figure 8 shows the average intensity values for a 20 A-scan region.

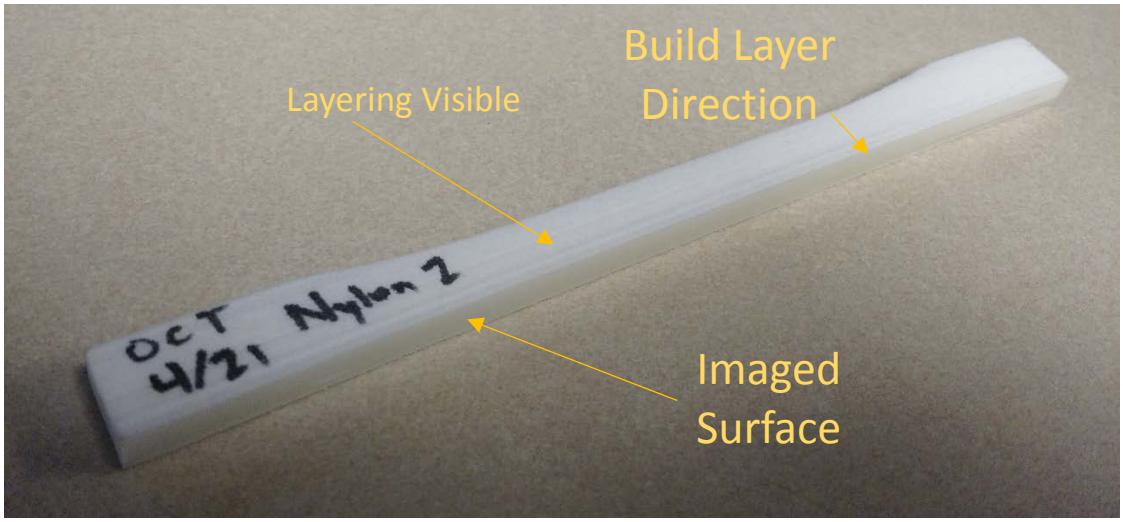

Figure 6: A Nylon 12, Layered Half Tensile Bar Specimen. The surface imaged with OCT was the vertical surface closest to the viewer.

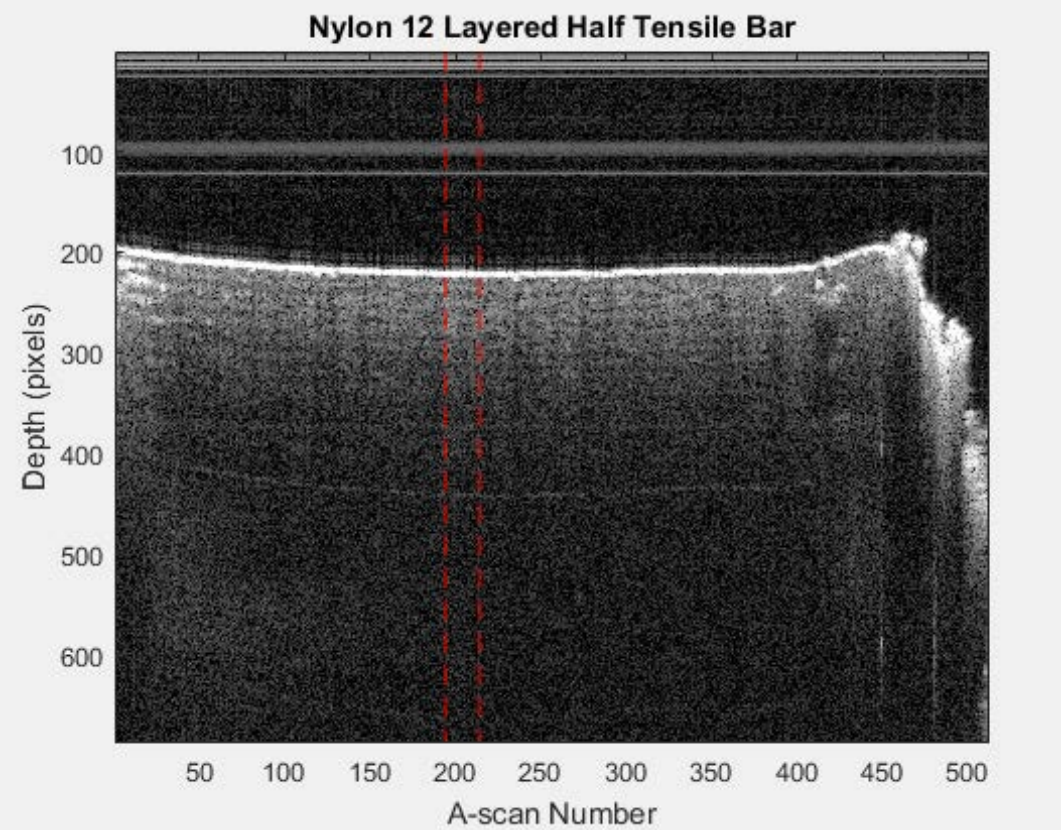

Figure 7: A single B-scan of the tensile bar is shown. Horizontal layers of bright intensity are visible just beneath the surface. The average intensities of the A-scans between the dotted lines are given in Figure 8.

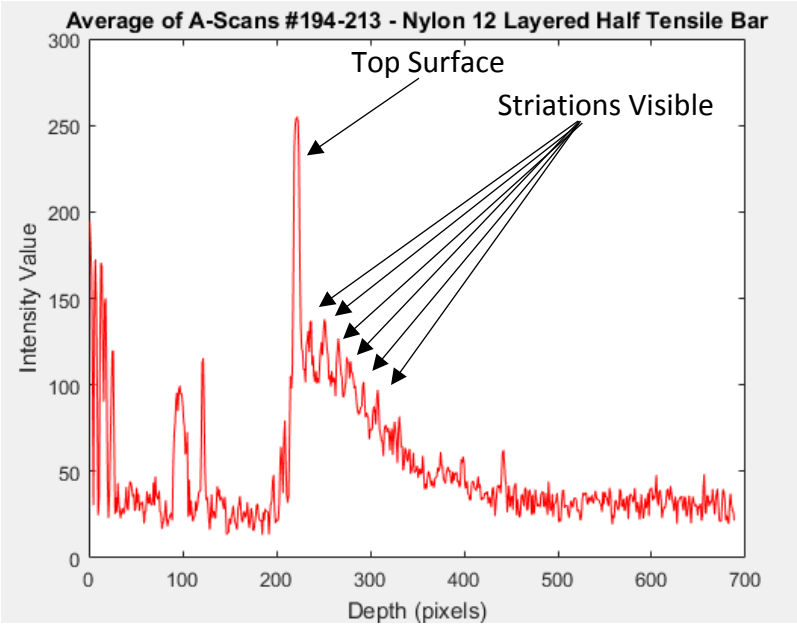

Figure 8: The average intensity of 20 consecutive A-scans is shown. The horizontal layering is evident after the surface peak. The averaging was performed to reduce the effect of noise.

In Figure 8, 6 somewhat regularly spaced striation peaks are present. It is thought that these striations correspond to the individual build layers, but additional analysis is required in order to confirm this.

PEEK Part with Noticeable Surface Pitting

A part made from polyether ether ketone (PEEK) with noticeable pitting on the surface was imaged next. Figure 9 shows a visual and OCT image of the PEEK part.

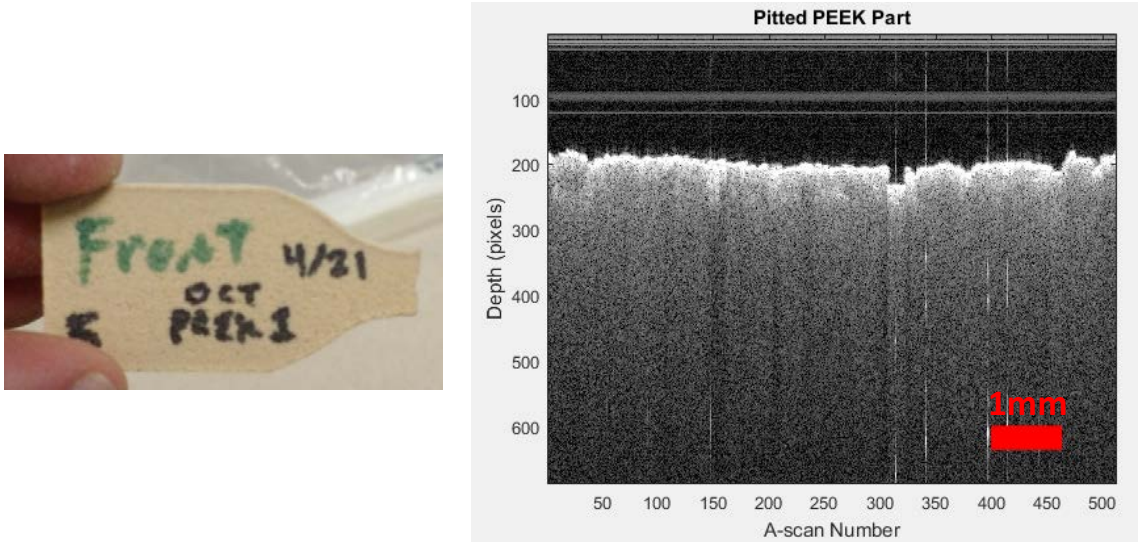

Figure 9: (Left) A visual image of a previously broken tensile bar made of PEEK powder with poor surface quality. (Right) Pits can be seen in surface quality. Potentially pits down to the size of 16 microns (the width represented by a single pixel) can be seen with the current OCT configuration.

In-Situ OCT: Experimental Setup

LAMPS Machine

The in-situ imaging of polymer powder and sintered material was done by installing an OCT system on the LAMPS machine. The LAMPS (Laser Additive Manufacturing Pilot System) machine was designed and built at The University of Texas at Austin as an open architecture SLS printer to allow increased monitoring and control of the process variables. The machine is outfitted with visual and infrared cameras and the ability to add and remove additional data acquisition elements (such as OCT) as needed. A more complete description of the LAMPS System can be found in Wroe et al. [8] and Fish et al. [9]. The right side of Figure 10 has been provided from Wroe et al. showing the LAMPS machine [8].

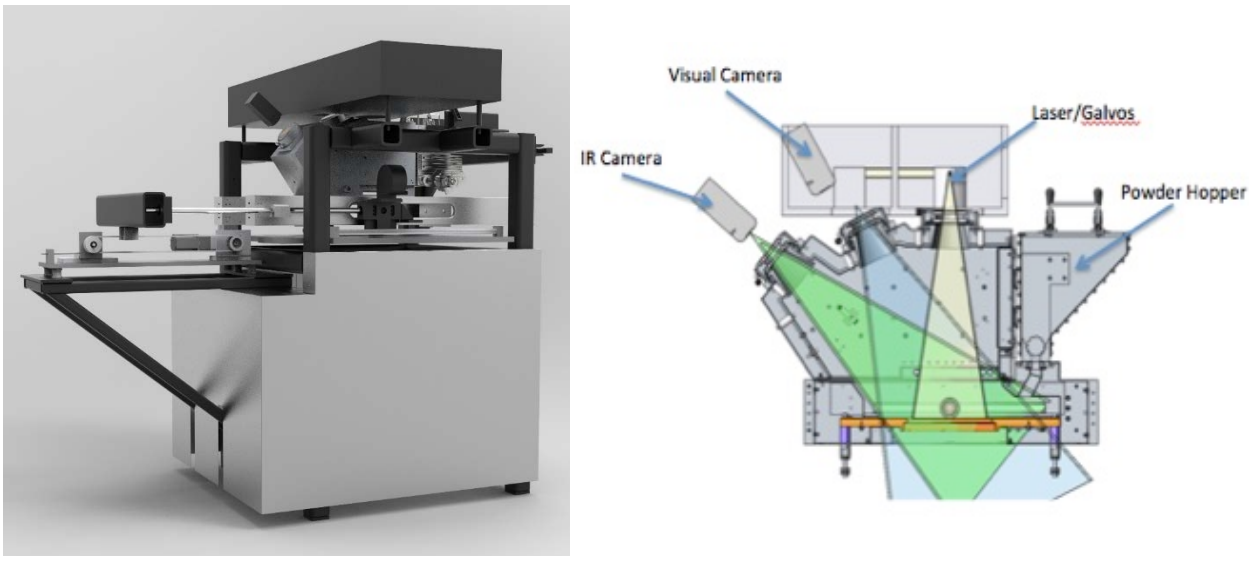

Figure 10 – (Left) External View of LAMPS CAD geometry (Right) LAMPS Build Chamber Cross Section

OCT Setup

For the in-situ OCT imaging, a 20 mW Santec HSL-2000 swept source laser with a central wavelength of 1310 nm and a sweep range of 60 nm at a scan rate of 20 kHz was used. The axial scan resolution is approximately 11 μm/pixel in air and the lateral resolution, with a necessarily long focal length lens, is approximately 186 μm/pixel. The optics of the LAMPS system were modified such that the OCT laser was boresighted with the CO_2 laser as shown in Figure 11.

This setup aligns the OCT beam to scan wherever the laser is pointing at all times. In actual implementation for this paper, the OCT beam scanned about 1 mm *behind* where the CO_2 laser was melting the surface powder.

The sample arm pathlength changes in relation to the reference arm pathlength based on where the CO_2 laser is pointing on the build surface. This causes the flat powder surface to appear curved in the OCT images. The longer path lengths farther from the center of the build area appear lower in the figures below. The OCT signal also weakens near the edges of the build area as the powder moves farther from the plane of best focus, however, both issues could be mitigated by using a field-flattening lens in the sample path. The present analysis was limited to data collection over a small region near the center of the build area so signal roll-off is not a major concern, but the flat powder surface does appear slightly curved in Figure 13 and Figure 15.

This boresighted OCT setup produced OCT images that were noisier than those produced from the ex-situ part analysis. This is because the long focal length lens in the boresighted OCT setup leads to a reduction in the solid angle of back reflected radiation coupled back into the system. In addition, the large spot size combined with the surface variation of the sample produced a reduced signal amplitude. Using a more powerful laser in the boresighted system would help to produce higher quality images in the boresighted setup in the future.

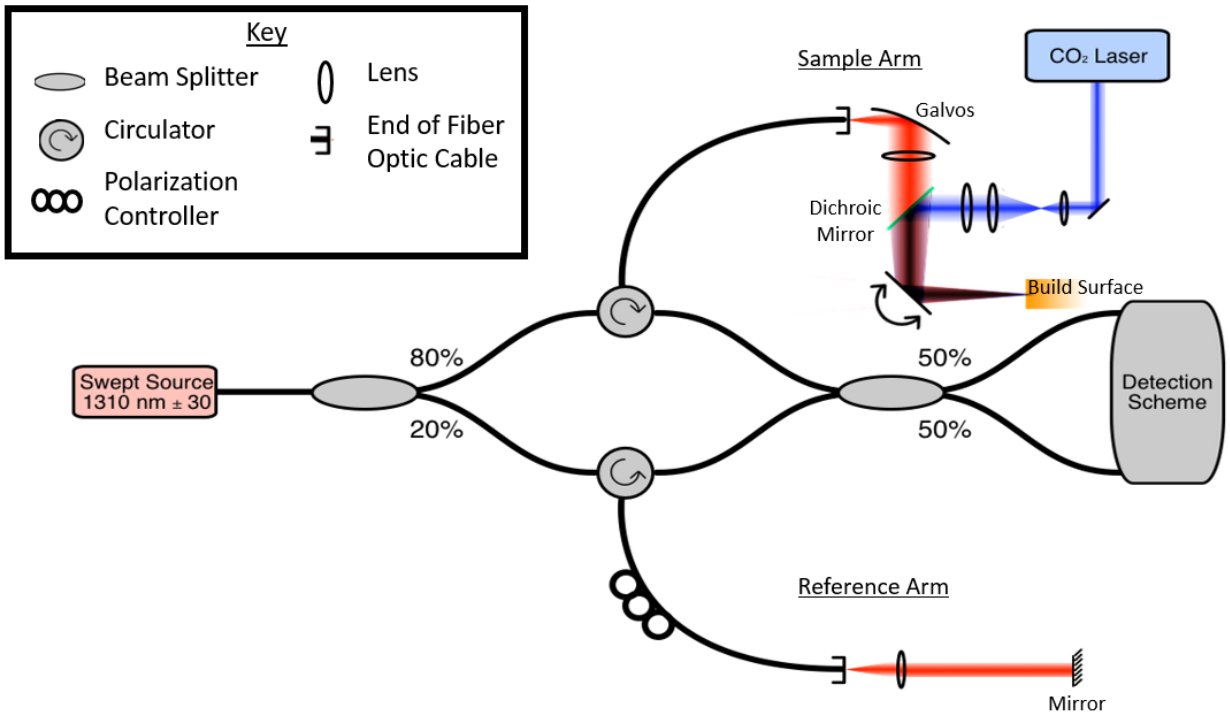

Figure 11 - Schematic of the Boresighted OCT Optics

In Situ OCT: Results

The in situ tests were run in the LAMPS machine using unrecycled polyamide 12 powder (PA 650, ALM). A single layer test designed to look at how a single scan line changes in time was run as well as a multilayer test looking at a few layers of sintered material.

Single Layer Scan Line

For this test, two markers were made approximately 4 cm apart by lasing a single point with 2.5 W for 0.1 seconds. This caused an easily recognizable divot in the surface of the powder. The marking holes were used to help identify the location of the OCT beam during post processing. Then, a pre-lase OCT scan was taken followed by the lasing of a 2.5 cm section in the middle of the two marking holes with the CO_2 laser. After lasing, the OCT beam was scanned back and forth across the freshly lased region and marking holes 100 times in about 3.2 seconds. This is shown in Figure 12. This test was run several times using different lasing powers.

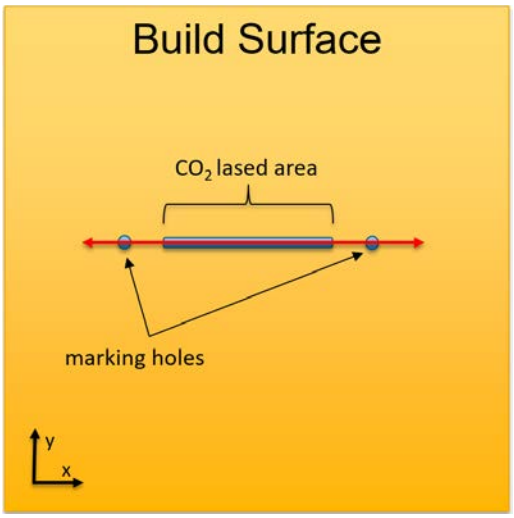

Figure 12: Diagram of the build surface from above for the single layer scan line test. First, two marking holes were made. Then, a single line was lased in between the two marking holes (blue area). Afterwards the OCT beam scanned back and forth (red arrow) over the marking holes and lased area 100 times in about 3.2 seconds.

The results from a high laser power, 32.5 W, are shown here. Although this is more than twice the laser power generally used during builds, the high laser power was able to accentuate some phenomena that are present, though less noticeable, at lower laser powers.

Figure 13 shows the pre and post-lasing OCT scans. Both images have had a non-local means de-noising filter applied [10]–[12]. The post-lase OCT image shows a melted region where the laser melted the powder together. The melted region itself is mostly transparent in the image. This makes sense because there are no interfaces in a pure liquid for radiation to reflect back from. However, the top liquid surface is clearly visible. The melted region is deeper on the right hand side. It was already known from previous work that a hot spot was created at the beginning of each scan line due to uneven heating while the laser accelerated. With OCT, the additional depth of the meltpool caused by overheating can be measured. This deeper melted region from the hot spot could be seen on a reduced scale at laser powers more typical of actual build conditions (not shown). The ghost line is an undesired effect of a piece of dust or other contaminant in the OCT system setup, causing a reflection which is not representative of the sample being imaged. This effect is local and is ignored in the present analysis.

Although the lower laser powers didn't produce a melt region as transparent as the one in Figure 13, they did show a region of reduced intensity. This can be seen in the multilayer test as well (see Figure 15).

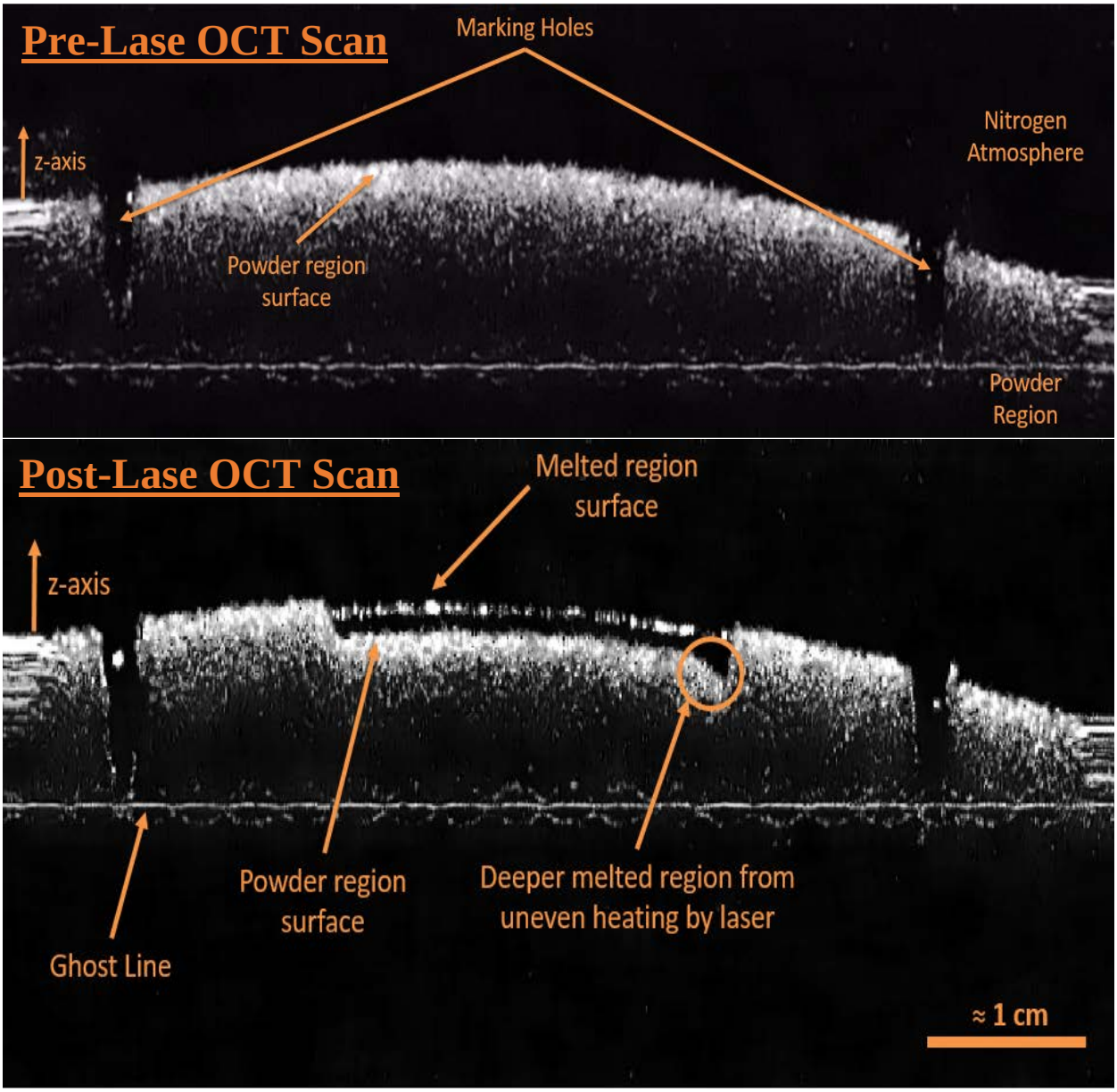

Figure 13: (Above) A single B-Scan of the test area before lasing with the CO2 laser. (Below) A B-scan of the test area 3.2 seconds after lasing with the CO2 laser.

Multilayer Scan Pattern

For the multilayer scan test, several layers of a 1" by 1" square were lased. In each layer, several marking holes were created, then a pre-lase OCT scan was performed followed by lasing of the square area, followed by a post-lase OCT scan. Between layers, a new layer of powder was dropped, heated to approximately 140°C and spread over the build surface. Figure 14 shows a diagram of a post-lase OCT scan for the multilayer test.

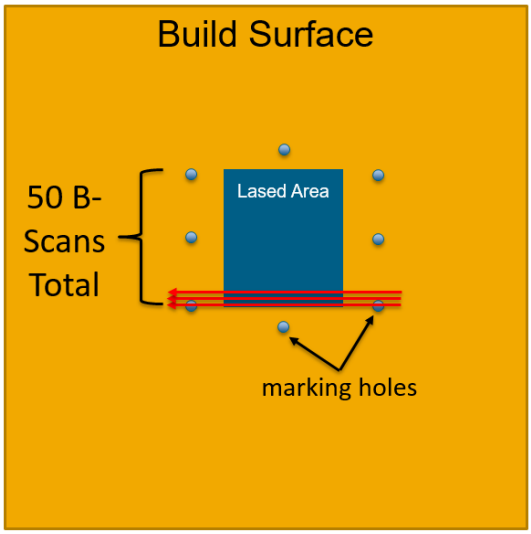

Figure 14 - Diagram of the build surface from above for a post-lase OCT scan of a single layer of the multilayer test. The marking holes and lased area are shown in blue. The first 3 OCT B-Scans are shown in red. 50 B-Scans make up each pre and post-lase OCT scan.

Figure 15 below shows corresponding B-scans on pre and post-lase OCT scans on the first layer as well as the post-lase OCT scan on the 2nd layer. The region that was lased lies in between the jump and mark delay regions. The jump and mark delays are brief pauses in laser movement after either a jump or a mark period respectively. Their original purpose is to ensure that the laser fires only on the intended area to be sintered. They produce readily recognizable regions where subsequent A-scans are relatively constant because the sensor is not moving and data is being duplicated in time.

In the 1st layer post-lase OCT scan (middle image), curling can be seen at the left of the lased region. The sintered layer also shows up as a reduced intensity layer on top of the un-sintered powder. In the 2nd layer post-lase OCT scan, the top 2 sintered layers are visible, although the boundary between the lower sintered layer and the un-sintered powder is not as defined as the boundary between the two sintered layers. The build failed after the 2nd layer due to part curl. The build was repeated at a reduced laser power and similar results were seen, but with layer interfaces being slightly less defined. Layers below the top 3 were not readily differentiated by visual inspection. This could likely be improved with a more powerful OCT laser.

Future Work

The fact that layers can be differentiated from each other and from un-sintered powder suggests that one could quantify the level of inter-layer bonding and perhaps predict where a part will fail. This will be analyzed in future work. Additionally, the fact that curling can be detected before the curl becomes severe enough to cause the build to fail indicates that it may be possible to correct a curl by using a lower laser power on the curling area or by adjusting the heating elements of the build chamber to reduce future curl. The LAMPS machine is ideally set up for both of these types of experiments and these will be examined in the future.

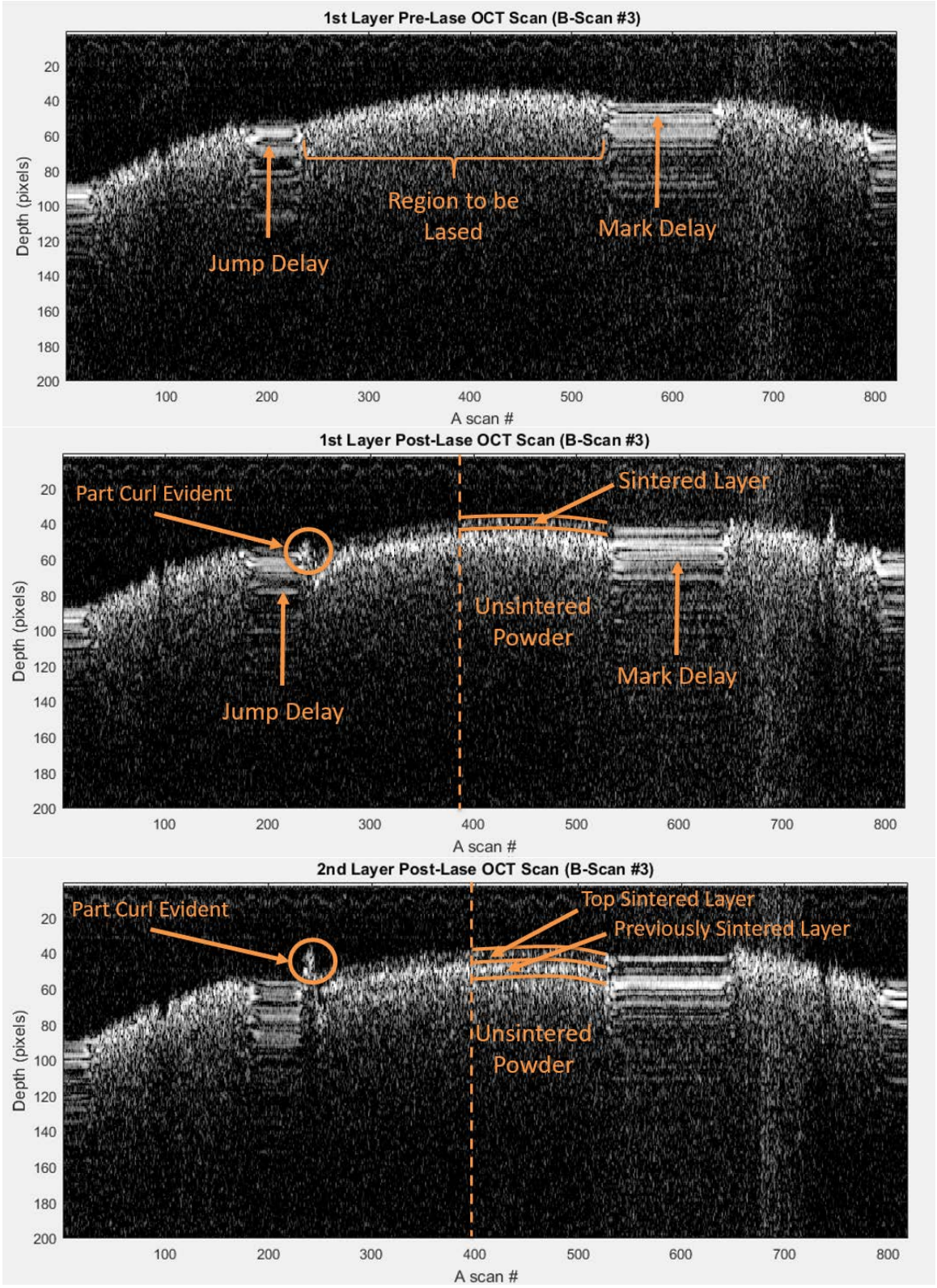

Figure 15 – Three corresponding B-Scans are shown. The individual layers as well as part curl are evident in the OCT images. (Top) 1st Layer Pre-Lase OCT Scan (Middle) 1st Layer Post-Lase OCT Scan (Bottom) 2nd Layer Post-Lase OCT Scan

Conclusion

The feasibility of OCT as a process monitoring tool was confirmed through ex situ analysis. Specifically, striations and surface roughness were observed in ex-situ part analysis. Then, for the first time an OCT system was bore sighted with the CO_2 laser on the LAMPS SLS machine and OCT data was taken of the powder and sintered material in-situ. It was observed that part curl can be detected before it causes the build to fail. Additionally, the top layers of the sintered material were resolved and differentiated from un-sintered powder.

Acknowledgements

The authors would like to acknowledge the instrumental research support of General Dynamics Information Technology, Inc. (GDIT) PO# 08ESM753983: Laser Additive Manufacturing - Pilot Scale System (LAMPS) (PI: Scott Fish); the Office of Naval Research (ONR) Award# N00014-12-1-0811/N00014-16-1-2393: Physics and Cyber-Enabled Manufacturing Process Control for Direct Digital Manufacture of Metal Parts (PI: Joseph Beaman); and the National Science Foundation (NSF) Award # CNS-1239343: CPS: Synergy: Cyber Enabled Manufacturing Systems for Small Lot Manufacture (PI: Joseph Beaman) for their support of this research.

References

[1] T. Wohlers, T. Caffrey, and R. I. Campbell, Wohlers Report 2016: 3d Printing and Additive Manufacturing State of the Industry, 1st ed. Fort Collins, Colorado: Wohlers Associates.
[2] I. Gibson, D. W. Rosen, and B. Stucker, Additive Manufacturing Technologies : Rapid Prototyping to Direct Digital Manufacturing. Boston: Springer, 2009.
[3] W. Drexler and J. G. Fujimoto, Optical coherence tomography: technology and applications, Second edition. Cham: SpringerReference, 2015.
[4] “Optical coherence tomography,” Wikipedia, the free encyclopedia. 25-Jun-2016.
[5] D. Stifter, “Beyond biomedicine: a review of alternative applications and developments for optical coherence tomography,” Appl. Phys. B, vol. 88, no. 3, pp. 337–357, Aug. 2007.
[6] G. Guan, Z. H. Lu, M. Hirsch, R. Goodridge, D. T. D. Childs, S. J. Matcher, A. T. Clare, and K. M. Groom, “Towards in-situ process monitoring in selective laser sintering using optical coherence tomography,” 2016, vol. 9738, p. 97380Q–97380Q–9.
[7] “Nylon 12.” [Online]. Available: http://polymerdatabase.com/polymers/nylon12.html. [Accessed: 06-Jul-2016].
[8] W. Wroe, J. Gladstone, T. Phillips, A. McElroy, S. Fish, and J. Beaman, “In-Situ Thermal Image Correlation with Mechanical Properties of Nylon-12 in SLS,” in Materials, Austin, TX, 2015.
[9] S. Fish, S. Kubiak, W. Wroe, J. Booth, A. Bryant, and J. Beaman, “A High Temperature Polymer Selective Laser Sintering Testbed for Controls Research,” in Process Development, Austin, TX, 2015.
[10] A. Buades, B. Coll, and J.-M. Morel, “Self-similarity-based image denoising,” Communications of the ACM, vol. 54, no. 5, pp. 109–117, May-2011.

[11] J. Darbon, A. Cunha, T. . Chan, S. Osher, and G. . Jensen, “Fast nonlocal filtering applied to electron cryomicroscopy,” in 2008 5th IEEE International Symposium on Biomedical Imaging: From Nano to Macro, 2008, pp. 1331–1334.
[12] T. Wagner and P. Behnel, ij-nl-means: Non local means 1.4.6 DOI: 10.5281/zenodo.47468. 2016.